Research Square

Preprints are preliminary reports that have not undergone peer review.
They should not be considered conclusive, used to inform clinical practice,
or referenced by the media as validated information.

Effect of TiO_2 nanotubes obtained from a Ti6Al4V alloy on the degradation of ciprofloxacin in aqueous solution by an electrochemical method

Laura Carolina Patiño Sánchez
Instituto Tecnológico Metropolitano: Instituto Tecnologico Metropolitano
Andrés Felipe Sanchez Medina
Instituto Tecnológico Metropolitano: Instituto Tecnologico Metropolitano
Robinson Aguirre Ocampo
Universidad de Antioquia
Carolina Ramirez Sánchez
Instituto Tecnológico Metropolitano: Instituto Tecnologico Metropolitano
Jasmin Porras
UNIREMINGTON Facultad de Ciencias de la Salud: Corporacion Universitaria Remington Facultad de Ciencias de la Salud
Manuel Romero-Sáez
Instituto Tecnológico Metropolitano: Instituto Tecnologico Metropolitano
Alejandro Alberto Zuleta Gil
UPB: Universidad Pontificia Bolivariana https://orcid.org/0000-0002-5431-2603
Jose Adrián Tamayo
josetamayo@itm.edu.co

Instituto Tecnológico Metropolitano: Instituto Tecnologico Metropolitano https://orcid.org/0000-0001-6095-957X

Research Article

Keywords: TiO2 nanotubes, Ti6Al4V, additive manufacturing, electrochemical anodization, emerging contaminants

Posted Date: November 24th, 2026

DOI: https://doi.org/10.21203/rs.3.rs-11569913/v1

License: This work is licensed under a Creative Commons Attribution 4.0 International License.
Read Full License

Abstract

The functional performance of anodic TiO_2 nanotube arrays depends on the relationship between their structural, chemical, and optical properties and their ability to support charge transfer. In this study, nanotubular oxide layers were formed by anodization on Ti6Al4V substrates manufactured by electron beam powder bed fusion (EB-PBF), and their electrochemical and photoelectrochemical behavior was evaluated. The nanotubes grew into a continuous layer approximately 850 nm thick, without delamination, with an average inner diameter of 59.79 ± 9.02 nm. Annealing at 350°C transformed the as-anodized amorphous oxide layer into the anatase phase. The anodic coating has a mixed-oxide structure in which alloy elements from the substrate modify optical absorption. The presence of Al_2O_3 and V_2O_5 species appears to shift the apparent bandgap to about 2.11 eV. The material showed no measurable photoelectrochemical activity under UV-C, simulated solar, or visible irradiation. Under galvanostatic polarization, the nanostructured electrode enabled approximately 49% removal of ciprofloxacin after 150 min, demonstrating its potential functionality under electrochemical treatment conditions. These findings show that anatase formation and an apparent optical absorption threshold in the visible range do not necessarily translate into measurable photoelectrochemical activation. The results highlight the need to assess optical properties alongside functional measurements when considering alloy-derived nanotubular oxides for water treatment applications.

1. Introduction

Anodic TiO_2 nanotube arrays have attracted interest as electrode materials for electrochemical and photoelectrochemical applications, including the removal of organic contaminants from water [1–3]. These structures combine the chemical stability of TiO_2 with a nanotubular architecture directly attached to a metallic substrate, facilitating their use as immobilized electrodes [4–6]. However, their functional performance depends not only on nanotube morphology but also on the composition, crystalline structure, and interfacial properties of the anodic layer, which influence charge generation, transport, and transfer [1, 7–9]. Therefore, the formation of an ordered nanotubular structure and favorable optical absorption does not necessarily ensure an efficient photoelectrochemical response. Understanding the relationship between these material properties and electrode behavior is essential for assessing their potential in water treatment applications.

In this context, the metallic substrate plays an important role in determining the characteristics of the anodic layer. Studies on Ti6Al4V have shown that electrolyte composition, anodization conditions and alloy microstructure, influence the growth and morphology of the resulting nanotubes [10, 11]. Unlike commercially pure Ti, Ti6Al4V contains alloying elements that can become incorporated into the oxide during anodization, producing a TiO_2-based layer containing Al and V derived species [3, 12]. These species can modify the optical and electrochemical properties of the nanotubes. Fraoucene et al.[12] reported an extension of optical absorption into the visible region in nanotube arrays obtained from Ti6Al4V, while Wang et al.[3] demonstrated visible-light photocatalytic activity in alloy-derived nanotubes with a double-walled architecture. These findings highlight the potential of Ti6Al4V as a substrate for

functional nanotubular oxides, while raising the need to examine how the composition and structure of the anodic layer relate to its electrochemical and photoelectrochemical behavior.

Electron beam powder bed fusion (EB-PBF) offers an additional opportunity for developing Ti6Al4V-based electrodes by allowing the fabrication of metallic substrates with tailored geometries. Previous studies have demonstrated the formation of ordered TiO_2 nanotube arrays on EB-PBF Ti6Al4V substrates [13] and shown that substrate orientation and processing route influence nanotube growth and electrochemical behavior [14]. These findings provide a basis for combining additive manufacturing with anodic surface modification in electrode development. However, assessing this approach for water treatment applications requires evaluating whether the resulting nanotubular layers exhibit suitable electrochemical and photoelectrochemical behavior.

Although previous studies have examined nanotube formation on EB-PBF Ti6Al4V substrates[13, 14] and the optical and photocatalytic properties of Ti6Al4V-derived oxides[3, 12] these findings do not establish whether the optical characteristics of nanotubular layers produced on EB-PBF substrates translate into a measurable photoelectrochemical response. Related research on anodized titanium alloys has shown that differences in photoinduced activity depend on oxide crystallinity and the electronic properties of the constituent oxides, indicating that the presence of a photoactive TiO_2 phase alone is insufficient to predict functional performance [8]. Addressing this question requires examining the structural and chemical characteristics of the anodic layer together with its behavior under illumination and electrical polarization. Such an assessment can help distinguish changes in optical absorption from effective photoinduced charge extraction and determine whether the material supports contaminant removal under externally imposed current.

Therefore, this study aims to evaluate the relationship between the material properties and the electrochemical and photoelectrochemical behavior of nanotubular oxide layers formed by anodization on Ti6Al4V substrates manufactured by EB-PBF. The morphology, crystalline structure, surface chemical composition, and optical properties of the annealed layers were characterized, and their response to illumination was examined through transient photocurrent measurements and electrochemical impedance spectroscopy. In addition, ciprofloxacin was used as a model organic contaminant to evaluate removal from aqueous solution under galvanostatic polarization. This approach provides an assessment of the functional capabilities and limitations of these electrodes for potential water treatment applications.

2. Experimental

2.1 Substrate fabrication and preparation

Electron beam powder bed fusion (EB-PBF) was employed to manufacture the Ti6Al4V substrates using an Arcam A2 electron beam melting (EBM) system (ARCAM, Mölndal, Västra Götaland, Sweden). The substrates were fabricated at an acceleration voltage of 60 kV, with a maximum beam power of 4 kW.

The process was conducted in a vacuum chamber (~ 10^{-4} mbar), at a build temperature between 600–700°C, and a deposited layer thickness of 50 µm [13, 14].

The fabricated specimens were sectioned using an Isomet 1000 precision cutter and mechanically polished using SiC abrasive papers of progressively finer grit sizes up to P1500. Prior to anodization, the samples were ultrasonically cleaned in acetone for 20 min, rinsed with deionized water, and dried in air.

2.2 Synthesis of TiO_2 nanotubes

TiO_2 nanotube arrays were synthesized via potentiostatic anodization in a two-electrode electrochemical cell. The EB-PBF Ti6Al4V substrate served as the anode, while a graphite bar served as the cathode. The organic electrolyte consisted of ethylene glycol containing 9 vol.% deionized water and 0.4 wt.% NH_4F. Anodization was performed at a constant potential of 30 V for 5000 s. After anodization, the samples were rinsed with ethanol and distilled water to remove residual electrolyte and minimize further chemical dissolution. To transform the as-anodized amorphous structure into the photoactive anatase phase, the samples were annealed at 350°C for 2 h in a muffle furnace, followed by natural cooling to room temperature [13, 14].

2.3 Characterization and analytical methods

The surface morphology and nanotubular architecture were examined by field emission scanning electron microscopy (FESEM). Cross-sectional observations were performed using focused ion beam-field emission scanning electron microscopy (FIB-FESEM) (Thermo Fisher Scientific Apreo 2). The elemental composition and distribution were analyzed by energy dispersive X-ray spectroscopy (EDS). The crystalline phases were investigated using a Horiba Jovin Yvon Raman spectrometer over the spectral range of 100 to 1000 cm^{-1}. The surface elemental composition of the specimens was determined by X-ray photoelectron spectroscopy (XPS) using a Thermo Scientific Scalab 250Xi under a vacuum of approximately 10^{-10} mbar, equipped with a monochromatic Al Kα X-Ray source (1486.7 eV, 13 kV). Binding energies were calibrated using the adventitious carbon C 1s peak at 285.0 eV as an internal reference to correct for charging effects. Spectral deconvolution and data processing were carried out using CasaXPS (Version 2.3.25PR1.0). The optical properties of the nanotubular oxide were evaluated by diffuse reflectance spectroscopy (DRS) using an Agilent Cary 100 UV-Vis Spectrophotometer, and the optical bandgap was estimated using the Kubelka–Munk transformation and Tauc plot analysis. The electrochemical behavior of the electrodes was investigated by transient photocurrent measurements and Electrochemical Impedance Spectroscopy (EIS) in a 3.5 wt.% NaCl, using an Ag/AgCl reference electrode.

2.4 Electrochemical degradation of ciprofloxacin

Electrochemical oxidation experiments were performed using ciprofloxacin (CIP) as a model organic compound. The experiments were carried out in an undivided glass cell containing 60 mL of a 0.06 mM CIP solution. A 10 mM KNO_3 solution was employed as the supporting electrolyte. The nanostructured Ti6Al4V electrode served as the working electrode, while a stainless-steel plate was used as the counter

electrode. When required, irradiation was provided by an LED source with a peak emission at 395 nm. The experiments were performed under galvanostatic conditions at a current density of 3 mA cm^{-2} with continuous magnetic stirring at 150 rpm. Aliquots were collected every 30 min for a total reaction time of 150 min and analyzed by high-performance liquid chromatography with diode-array detection (HPLC-DAD) to determine the residual ciprofloxacin concentration.

3. Results

3.1 Morphological characterization

Anodization of the EB-PBF Ti6Al4V substrate resulted in the formation of self-organized TiO_2 nanotube arrays. The surface and cross-sectional morphology were examined by FESEM. The top view (Fig. 1a) shows a homogeneous nanotubular architecture composed of open-ended pores arranged in a characteristic honeycomb-like pattern. The nanotubes exhibited an average inner diameter of 59.79 ± 9.02 nm, which is consistent with the nanotube dimensions typically obtained at an anodization potential of 30 V [5, 6]. The cross-sectional image (Fig. 1b) reveals that the nanotubes grew perpendicular to the substrate surface, forming a continuous oxide layer. No evidence of delamination, interfacial cracking, or structural discontinuities was observed along the nanotube/substrate interface [13].

The crystalline structure of the nanotubular layer was evaluated by Raman spectroscopy before and after thermal annealing. The as-anodized sample (Fig. 2a) exhibited a broad featureless spectrum without well-defined vibrational bands, indicating that the oxide layer was predominantly amorphous or poorly crystalline [13, 14]. After annealing (Fig. 2b) five characteristic Raman bands appeared at 144, 197, 399, 516, and 639 cm^{-1}, corresponding to the Eg(1), Eg(2), B1g(1), A1g/B1g(2), and Eg(3) vibrational modes of anatase TiO_2, respectively [7, 14]. Among these, the Eg (1) mode at 144 cm^{-1} exhibited the highest relative intensity, confirming the successful crystallization of the nanotubular oxide into the anatase phase.

The elemental distribution across the nanotubular layer was investigated by cross-sectional EDS line-scan analysis. The elemental profile was acquired from the top surface of the nanotubes toward the Ti6Al4V substrate, as illustrated in Fig. 3a. Within the nanotubular region, the EDS analysis exhibits a strong oxygen signal, together with titanium, consistent with the formation of a TiO_2-based anodic oxide (Fig. 3b). A sharp compositional transition was observed at approximately 850 nm, defining the interface between the nanotubular layer and the metallic substrate [5, 6]. In addition, vanadium was detected throughout the nanotubular oxide, with a noticeable enrichment between approximately 500 and 850 nm (Fig. 3c), indicating that alloying elements from the substrate were incorporated into the anodic oxide during anodization [11, 12].

Figure 4 presents the XPS spectra of the anodized samples. The Al 2p spectrum (Fig. 4a) consists of two clearly separated contributions. The peak at 73.75 eV is assigned to Al-O bonding; the second peak at 74.72 eV is related to Al-OH bonding [15–17]. The Ti 2p region (Fig. 4b) was deconvoluted into one pair

of spin-orbit doublets. The doublet exhibited peaks at 458.57 eV (Ti 2p3/2) and 464.30 eV (Ti 2p1/2) with a spin-orbit splitting of 5.7 eV, is indicative of Ti-O bonds in Ti^{4+} species[18] The V 2p region (Fig. 4c) was deconvoluted into one spin-orbit doublet. This doublet features peaks at 517.10 eV (V 2p3/2) and 524.49 eV (V 2p1/2), with a spin-orbit splitting of 7.4 eV, indicating the presence of V-O bonds in V^{5+} species [18, 19]. The O 1s region (Fig. 4d) shows two clearly separated contributions; the primary peak at 530.01 eV is attributed to lattice oxygen (O^{2-}) in TiO_2, Al_2O_3, and V_2O_5. The component at 531.45 eV is assigned to Al-OH bonding [20].

Diffuse reflectance spectroscopy (DRS) was employed to evaluate the optical properties and bandgap of the anodic TiO_2 nanotubular layer. The apparent optical bandgap (Eg) was estimated using the Kubelka–Munk transformation and Tauc plot analysis (Fig. 5). The bandgap energy was obtained by extrapolating the linear region of the $(F(R)h\nu)^2$ vs. photon energy ($h\nu$) plot to the energy axis, where F(R) is the Kubelka-Munk function derived from the diffuse reflectance spectrum.

The anodic mixed oxide exhibits an apparent optical bandgap of approximately 2.11 eV, which is considerably lower than the bandgap commonly reported for pure TiO_2 (3.2–3.4 eV) [12]. This result indicates that anodization of the EB-PBF Ti6Al4V alloy produced a nanotubular oxide with optical properties that differ from those of conventional anatase TiO_2.

Transient photocurrent measurements were performed under UV-C, simulated solar, and visible-light irradiation to evaluate the photoelectrochemical response of the anodic nanotubular oxide (Fig. 6a-c). Under all irradiation conditions, the electrodes exhibited a relatively high initial current that rapidly decreased during the first seconds of the experiment, followed by a quasi-steady current with low-amplitude fluctuations. Repeated illumination cycles did not produce the characteristic step-like current response typically associated with efficient photogenerated charge separation, and no reproducible increase in current was observed upon light irradiation.

In addition, the Nyquist plots recorded under illuminated and dark conditions (Fig. 6d) nearly overlapped, indicating that irradiation did not significantly modify the interfacial electrochemical response of the electrode. Therefore, under the evaluated conditions, the annealed Ti6Al4V NT electrode did not exhibit measurable photoelectrochemical activation.

Figure 7 shows the evolution of the normalized ciprofloxacin concentration during electrochemical treatment using annealed Ti6Al4V NT electrodes under galvanostatic conditions at 3 mA cm^{-2} in 10 mM KNO_3, with an initial ciprofloxacin concentration of 0.06 mM. The normalized concentration showed an overall decrease from $C_i/C_0 = 1$ to approximately 0.51 after 150 min, corresponding to approximately 49% ciprofloxacin removal. The concentration decreased more markedly during the first 60 min, followed by a slower overall decrease during the remaining reaction time, with a slight fluctuation observed around 90 min. Since the concentration was quantified by HPLC, this decrease represents a reduction in the concentration of the parent ciprofloxacin compound, as determined from its chromatographic response [2].

4. Discussion

The morphological and structural characterization demonstrated that anodization successfully produced a continuous and vertically aligned Ti6Al4V-based nanotubular layer. The dimensions and overall morphology of the nanotubes are consistent with previous reports for anodized Ti6Al4V, particularly for substrates manufactured by EB-PBF or processed by conventional routes [13, 14]. However, the growth of nanotubes on Ti6Al4V is more complex than on commercially pure Ti because of the α + β phase microstructure of the alloy. Ribeiro et al. [21] demonstrated that the α phase, which is Al-stabilized, and the β phase, which is V-rich, exhibit different electrochemical reactivities during anodization. The higher Al content in the α phase promotes repassivation, whereas the higher solubility of V-rich oxides favors earlier pore formation in β region [21]. Therefore, the slight variations observed in nanotube diameter and morphology are likely associated with local differences in oxide formation and dissolution across the alloy microstructure.

The Raman analysis confirmed that the as-anodized nanotubular layer was initially amorphous or poorly crystalline and that annealing induced crystallization into anatase TiO_2. This structural transformation is generally regarded as a prerequisite for improving charge transport, since the ordered anatase lattice reduces structural disorder and facilitates carrier mobility compared with amorphous TiO_2. Moreover, previous studies have shown that the degree of anatase crystallinity and crystal orientation can influence electron transport and photoelectrochemical performance in TiO_2 nanotube arrays [7]. Nevertheless, the results of this work show that the crystallization into anatase alone was insufficient to produce a measurable photoelectrochemical response. This suggests that additional factors, including the mixed-oxide composition, defect chemistry, charge trapping, electron–hole recombination, and interfacial charge-transfer resistance, play a dominant role in determining the functional behavior of the nanotubular oxide.

The EDS line scan revealed that the anodic nanotubular layer was not composed solely of TiO_2 but also contained alloying elements originating from the Ti6Al4V substrate. The layer therefore be regarded as a TiO_2-based mixed oxide rather than pure TiO_2. This agrees with reports made by Fraoucene *et al.* [12] and Wang *et al.* [3], who detected alloying elements in Ti6Al4V nanotube arrays and associated them with changes in optical and functional properties.

The optical characterization of the Ti6Al4V NTs supports the view that the incorporation of alloying elements modifies the electronic structure of the anodic nanotubular oxide. The marked reduction in the apparent optical bandgap suggests that alloy-derived species modify the electronic structure of the anodic oxide, either by introducing additional electronic states within the band gap or through the formation of mixed-oxide phases. Fraoucene *et al.* [12] reported a similar shift for Ti6Al4V-derived TiO_2 nanotubes and attributed the reduction in the apparent optical bandgap to vanadium oxide. Wang *et al*. [3] also reported that V_2O_5 generated from Ti6Al4V can dominate the visible-light response of double-walled alloy titanium dioxide nanotube arrays. Therefore, the combined EDS and DRS results suggest that the incorporation of alloying elements, particularly vanadium-derived oxide species, plays a major

role in modifying the optical response of the anodic nanotubular layer. The incorporation of vanadium into the nanotubular oxide was evidenced by cross-sectional EDS analysis, while the XPS results indicated the presence of V species, consistent with V_2O_5-like chemical environments.

However, the bandgap narrowing did not translate into a clear photoelectrochemical response. The photocurrent measurements under UV-C, solar, and visible irradiation did not show a reproducible increase in current, and the ON/OFF EIS spectra were nearly identical. This indicates that the optical absorption observed in the Ti6Al4V NT was not enough to promote efficient charge separation, transport, and extraction. If photon energy were the only limitation, UV-C irradiation should have generated a measurable response because its photon energy is sufficient to excite anatase TiO_2. The absence of photoelectrochemical activity even under UV-C suggests that the limiting processes are more likely related to charge recombination, trapping, poor electronic connectivity, barrier-layer resistance, or unfavorable mixed-oxide interfaces.

This behavior may be associated with the antagonistic role of alloying-element oxides. Vanadium-containing species may reduce the apparent bandgap and extend light absorption toward lower energies, but the same electronic states may also act as trap states or recombination centers. Also, aluminum-containing oxide domains, likely associated with Al_2O_3-like regions, may behave as insulating barriers because Al_2O_3 has a wide bandgap and low electronic conductivity. Thus, the alloying elements can simultaneously modify the optical absorption of the nanotubular layer and hinder electron transport through it. This explains why Ti6Al4V NTs may show a bandgap shift while failing to produce a measurable photocurrent under the evaluated irradiation conditions. Similar limitations have been reported in anodized Ti alloy systems, where recombination and the electronic structure of alloying-element oxides can strongly affect the final photoinduced activity [8].

The EIS results reinforce this interpretation. In an efficient photoelectrode, illumination would be expected to modify the interfacial impedance because photogenerated carriers participate in charge-transfer reactions at the electrode/electrolyte interface. In this case, the overlap between ON and OFF spectra indicates that illumination did not significantly alter charge-transfer resistance or interfacial behavior. Therefore, photogenerated carriers, if produced, were probably lost through recombination or trapped within the mixed oxide structure before contributing to measurable current or interfacial reactions.

Although the annealed Ti6Al4V NT electrode did not show a measurable photoelectrochemical response under the evaluated irradiation conditions, it enabled approximately 49% ciprofloxacin removal after 150 min under electrochemical galvanostatic polarization at 3 mA cm^{-2} (Fig. 7). This result demonstrates the functional performance of the nanostructured electrode under electrochemical treatment conditions, despite its limited photoelectrochemical response. Since the reaction driving ciprofloxacin removal are sustained by the externally applied current rather than by photogenerated carriers, the limitations affecting photoinduced charge separation and transport do not prevent charge transfer at the electrode–electrolyte interface. This distinction agrees with the broader understanding of TiO_2 nanotube electrodes

as binder-free platforms for electrochemical and photoelectrochemical reactions, whose performance depends strongly on charge-transfer resistance, band structure, and surface/interface properties [9].

The use of 10 mM KNO_3 as supporting electrolyte is also relevant because it provides ionic conductivity without the addition of chloride ions, thereby avoiding oxidation pathways associated with electrogenerated active chlorine species. Possible oxidation pathways include direct electron transfer at the electrode surface and indirect reactions involving electrochemically generated oxidizing species [22]. However, in the absence of comparative experiments performed under electrochemical-only and irradiation-only conditions, the relative contributions of these pathways cannot be distinguished. Since HPLC was used to quantify the concentration, the observed decrease demonstrates removal of the parent ciprofloxacin compound but does not establish complete mineralization or identify the transformation products formed during treatment.

From a materials perspective, these findings demonstrate the functional applicability of EB-PBF Ti6Al4V electrodes modified with anodic TiO_2 nanotubes under electrochemical conditions. The ciprofloxacin removal experiment therefore provides a proof of concept for the potential use of this nanostructured material in electrochemical water treatment. Although the removal achieved under the present conditions was moderated (~ 49%), the use of EB-PBF substrates offers an additional advantage from an application perspective. Additive manufacturing enables the fabrication of Ti6Al4V electrodes with tailored geometries that can be functionalized by anodization, providing design flexibility to adapt the electrode to different reactor configurations. This adaptability could allow these electrodes to be integrated as a pretreatment stage within combined treatment schemes, complementing other removal processes. Nevertheless, further experiments, including comparisons with unmodified Ti6Al4V substrates and appropriate electrochemical and photochemical controls, would be necessary to establish the specific contribution of the nanotubular oxide and clarify the underlying reaction mechanisms.

Conclusions

TiO_2 nanotube arrays were grown by anodization on Ti6Al4V substrates manufactured by EB-PBF. They formed a continuous layer with a thickness of approximately 850 nm, without delamination, with an average inner diameter of 59.79 ± 9.02 nm. Annealing at 350°C crystallized the as-anodized amorphous oxide into anatase. The anodic layer has a mixed-oxide structure in which alloying elements from the substrate modify optical absorption but limit photoinduced charge extraction. The presence of Al_2O_3 and V_2O_5 species appear to shift the apparent bandgap to about 2.11 eV, and may simultaneously introduce recombination centers, electron traps, or local transport barriers. Consequently, the material showed no measurable photoelectrochemical activity under UV-C, simulated solar, or visible irradiation. The absence of a measurable photoelectrochemical response even under UV-C irradiation suggests that charge separation, recombination, and/or transport limitations may contribute to the observed behavior. Nevertheless, under galvanostatic polarization the TiO_2-functionalized Ti6Al4V electrode enabled

approximately 49% CIP removal after 150 min. This result demonstrates the potential of the nanostructured material for electrochemical applications, although further studies are required to distinguish the contributions of electrochemical oxidation pathways. Furthermore, since EB-PBF enables the fabrication onf Ti6Al4V electrodes with tailored geometries that can be subsequently functionalized by anodization, this approach offers design flexibility for integrating these electrodes as a pretreatment stage within combined water treatment schemes.

Declarations

Conflicts of interest/Competing interests

The authors declare that they have no known competing financial interests or personal relationships that could have appeared to influence the work reported in this manuscript.

Funding

The authors declare that no funds, grants, or other financial support were received for the conduct of this study.

Authors’ contributions

Jose Adrián Tamayo and Carolina Ramírez-Sánchez contributed to the conceptualization of the study and formulation of the research objectives. Alejandro Zuleta, Carolina Ramírez-Sánchez, Jasmín Porras, and Jose Adrián Tamayo developed the methodology and established the experimental and analytical procedures. Robinson Aguirre Ocampo performed the formal analysis and contributed to the interpretation of the results. Laura Carolina Patiño and Andrés Felipe Sánchez-Medina conducted the experimental investigation and collected the data. The original draft of the manuscript was prepared by Robinson Aguirre Ocampo and Laura Carolina Patiño. Jose Adrián Tamayo and Manuel Romero-Sáez critically reviewed and edited the manuscript. Laura Carolina Patiño, Robinson Aguirre Ocampo, and Jose Adrián Tamayo contributed to the preparation of figures and data visualization. Jose Adrián Tamayo and Carolina Ramírez-Sánchez supervised the research and were responsible for funding acquisition. All authors read and approved the final version of the manuscript.

Acknowledgements

The authors would like to thank Institución Universitaria ITM, Universidad de Antioquia, Universidad Pontificia Bolivariana, and Corporación Universitaria Remington for providing access to laboratory facilities, equipment, and technical infrastructure that supported the development of this research.

References

1. Martín de Vidales MJ, Prieto R, Galán-Lucarelli G et al (2023) Removal of contaminants of emerging concern by photocatalysis with a highly ordered TiO2 nanotubular array catalyst. Catal Today ; 413–415: 113995
2. Liu L, Li R, Liu Y et al (2016) Simultaneous degradation of ofloxacin and recovery of Cu(II) by photoelectrocatalysis with highly ordered TiO2 nanotubes. J Hazard Mater 308:264–275
3. Wang Y, Zhang X, You S et al (2020) One-step electrosynthesis of visible light responsive double-walled alloy titanium dioxide nanotube arrays for use in photocatalytic degradation of dibutyl phthalate. RSC Adv 10:21238–21247
4. Macák JM, Tsuchiya H, Schmuki P (2005) High-aspect-ratio TiO2 nanotubes by anodization of titanium. Angew Chem Int Ed 44:2100–2102
5. Roy P, Berger S, Schmuki P (2011) TiO2 nanotubes: Synthesis and applications. Angew Chem Int Ed 50:2904–2939
6. Regonini D, Bowen CR, Jaroenworaluck A et al (2013) A review of growth mechanism, structure and crystallinity of anodized TiO2 nanotubes. Mater Sci Engineering: R: Rep 74:377–406
7. Sierra-Uribe H, Córdoba-Tuta EM, Acevedo-Peña P (2017) The Effect of the Heating Rate on Anatase Crystal Orientation and Its Impact on the Photoelectrocatalytic Performance of TiO 2 Nanotube Arrays. J Electrochem Soc 164:H279–H285
8. Masahashi N, Hatakeyama M, Mori Y et al Photoinduced properties of anodized Ti alloys for biomaterial applications. *Sci Rep*; 13. Epub ahead of print 1 December 2023. 10.1038/s41598-023-41189-z
9. Yoo H, Kim M, Kim YT et al Catalyst-doped anodic TiO2 nanotubes: Binder-free electrodes for (photo)electrochemical reactions. *Catalysts*; 8. Epub ahead of print 17 November 2018. 10.3390/catal8110555
10. Matykina E, Conde A, De Damborenea J et al (2011) Growth of TiO2-based nanotubes on Ti–6Al–4V alloy. Electrochim Acta 56:9209–9218
11. Ribeiro B, Offoiach R, Rossetti S et al (2022) On Growth and Morphology of TiO2 Nanotubes on CP-Ti by Anodic Oxidation in Ethylene Glycol Electrolyte: Influence of Electrolyte Aging and Anodization Parameters. Mater 2022 15:15: 3338
12. Fraoucene H, Sugiawati VA, Hatem D et al Optical and electrochemical properties of self-organized TiO2 nanotube arrays from anodized Ti-6Al-4V alloy. Front Chem ; 7. Epub ahead of print 2019. 10.3389/fchem.2019.00066
13. Ocampo RA, Bedoya Ochoa N, Tamayo JA et al (2023) Formation of highly ordered TiO2 nanotubes on Ti6Al4V alloys manufactured by electron beam powder bed fusion (E-PBF). Int J Adv Manuf Technol 128:257–266
14. Vásquez FA, Aguirre Ocampo R, Bedoya N et al (2025) Electrochemical characterization of TiO2 nanotubes formed on Ti6Al4V manufactured by PBF-EB or forging. Progress Additive Manuf

10:3629–3639

15. Usman M, Arshad M, Suvanam SS et al (2018) Influence of annealing environment on the ALD-Al2O3/4H-SiC interface studied through XPS. J Phys D Appl Phys 51:105111
16. Fang R-C, Sun Q-Q, Zhou P et al (2013) High-performance bilayer flexible resistive random access memory based on low-temperature thermal atomic layer deposition. *Nanoscale Research Letters* ; 8: 92-
17. Hoque E, Derose JA, Kulik G et al (2006) Alkylphosphonate Modified Aluminum Oxide Surfaces. J Phys Chem B 110:10855–10861
18. Biesinger MC, Lau LWM, Gerson AR et al (2010) Resolving surface chemical states in XPS analysis of first row transition metals, oxides and hydroxides: Sc, Ti, V, Cu and Zn. Appl Surf Sci 257:887–898
19. Silversmit G, Depla D, Poelman H et al (2004) Determination of the V2p XPS binding energies for different vanadium oxidation states (V5 + to V0+). J Electron Spectros Relat Phenom 135:167–175
20. Muñoz L, Tamayo L, Gulppi M et al (2018) Surface Functionalization of an Aluminum Alloy to Generate an Antibiofilm Coating Based on Poly(Methyl Methacrylate) and Silver Nanoparticles. *Molecules*; 23. Epub ahead of print 24 October 10.3390/MOLECULES23112747
21. Ribeiro B, Offoiach R, Rahimi E et al (2021) On Growth and Morphology of TiO2 Nanotubes on Ti6Al4V by Anodic Oxidation in Ethylene Glycol Electrolyte: Influence of Microstructure and Anodization Parameters. Mater 2021 14:14: 2540
22. Yuan Q, Qu S, Li R et al (2023) Degradation of antibiotics by electrochemical advanced oxidation processes (EAOPs): Performance, mechanisms, and perspectives. Sci Total Environ 856:159092

Figures

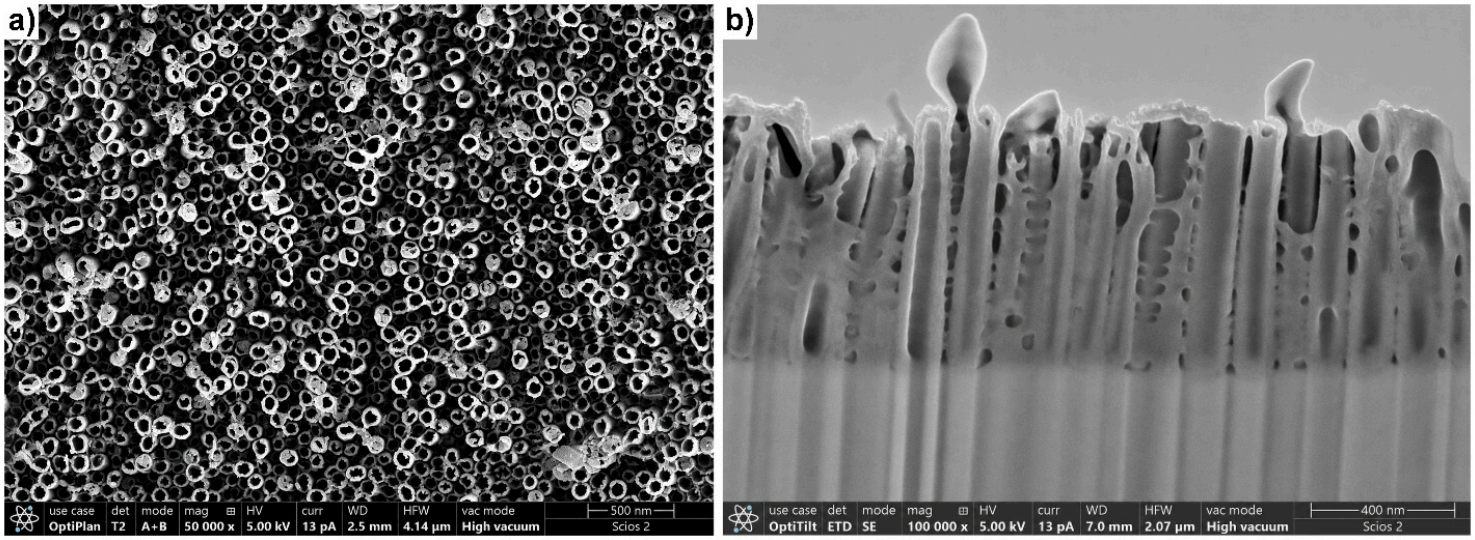


Figure 1

FESEM micrographs of TiO_2 nanotubes formed on Ti6Al4V substrates manufactured by EB-PBF.

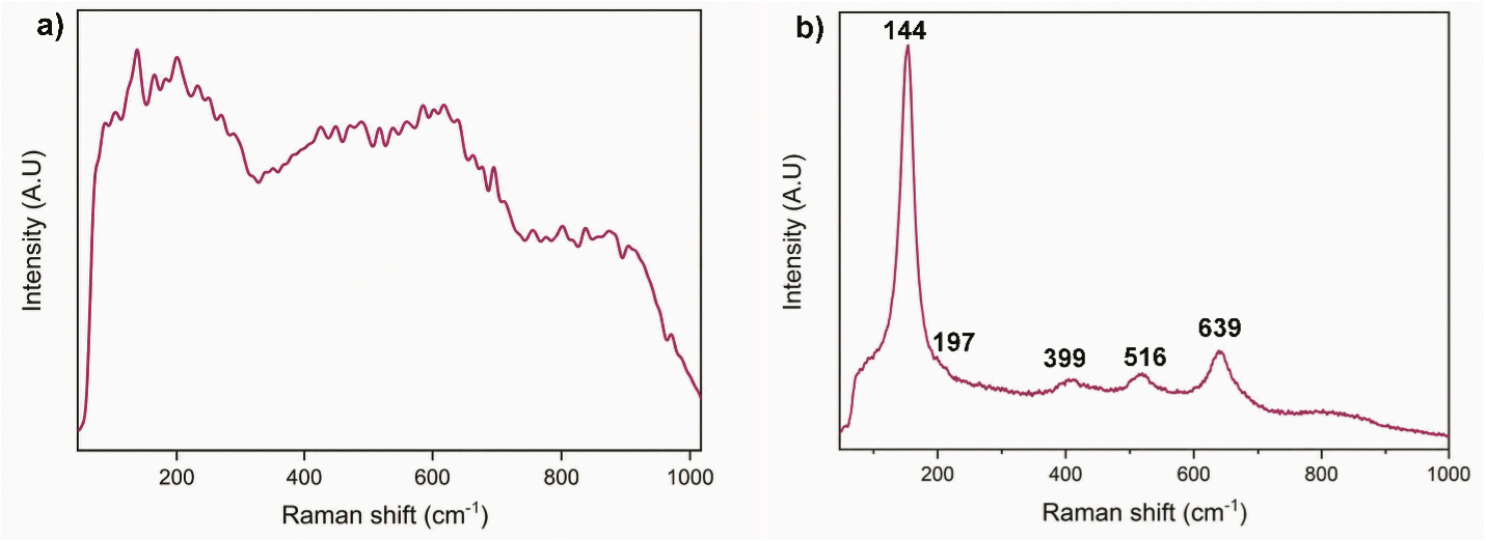


Figure 2

Raman spectra of the anodic oxide layer a) before and b) after thermal annealing.

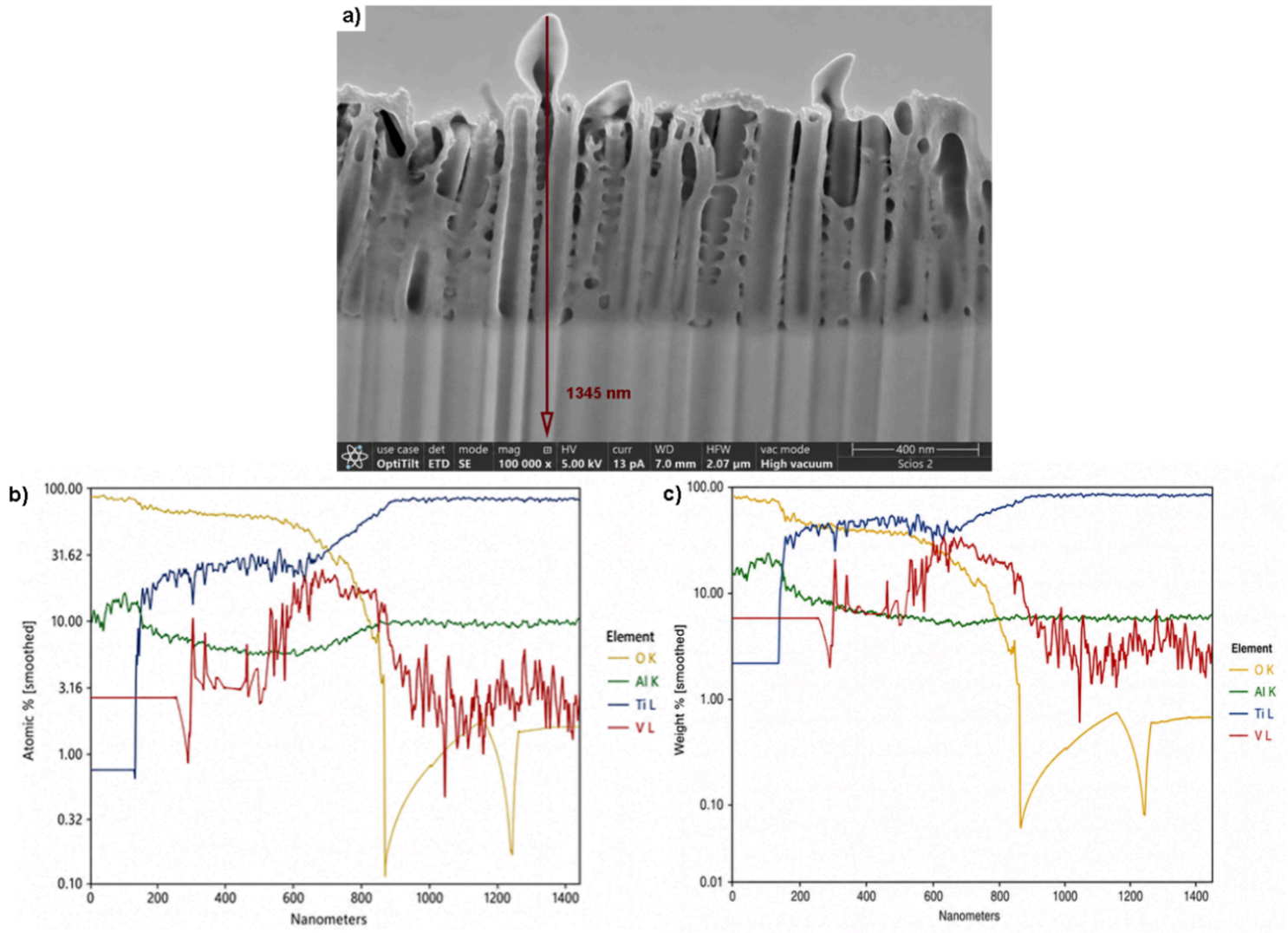


Figure 3

Cross-sectional EDS line-scan analysis of the anodized Ti6Al4V substrate where b) represents the atomic percentage, and c) the weight percentage of each element of the alloy.

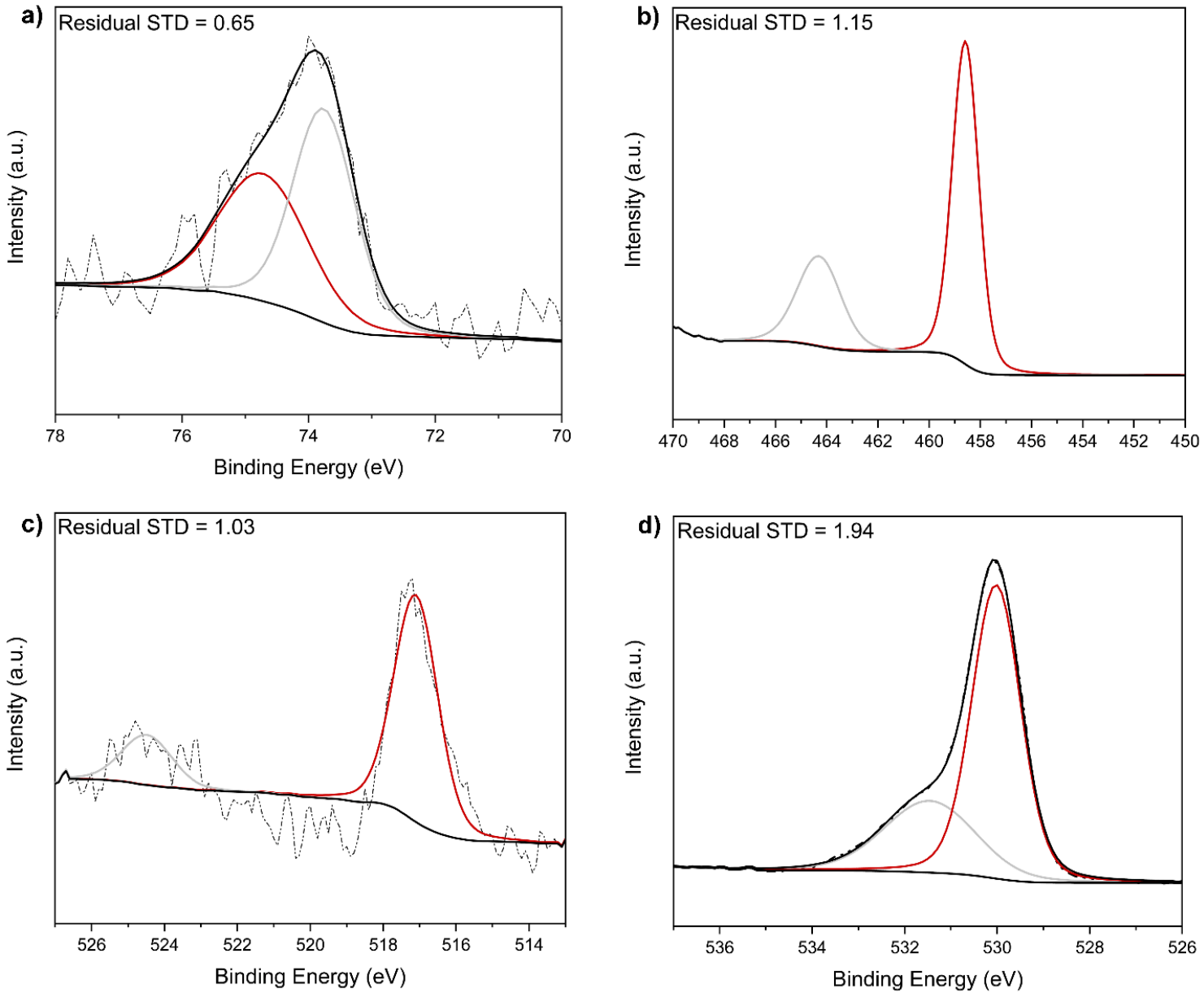


Figure 4

XPS spectra of the anodized samples, (a) Al 2p region (b) Ti 2p region (c) V 2p region and (d) O 1s region.

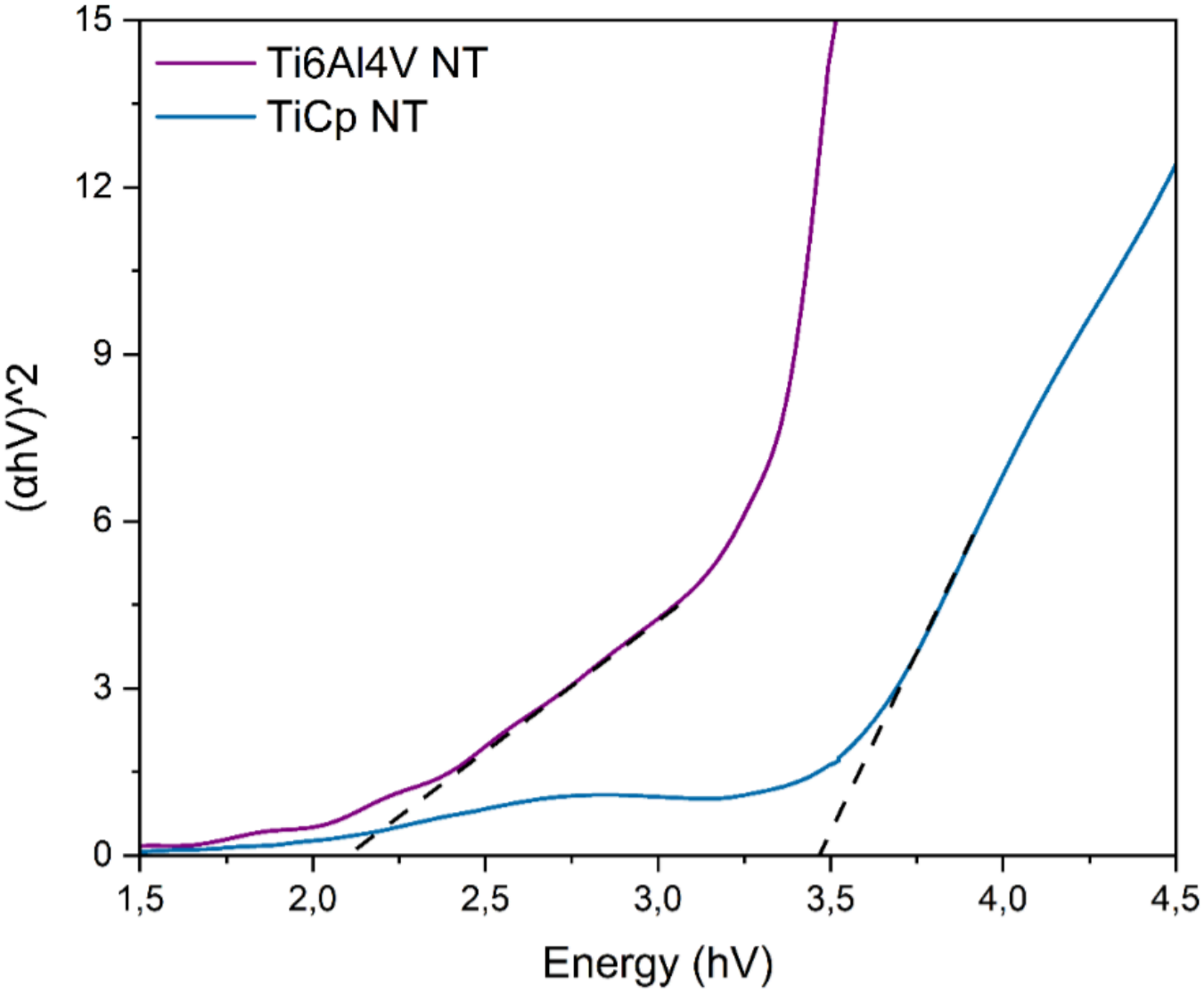


Figure 5

Tauc plots obtained from diffuse reflectance measurements of TiO_2 nanotube arrays formed on Ti6Al4V and commercially pure Ti substrates.

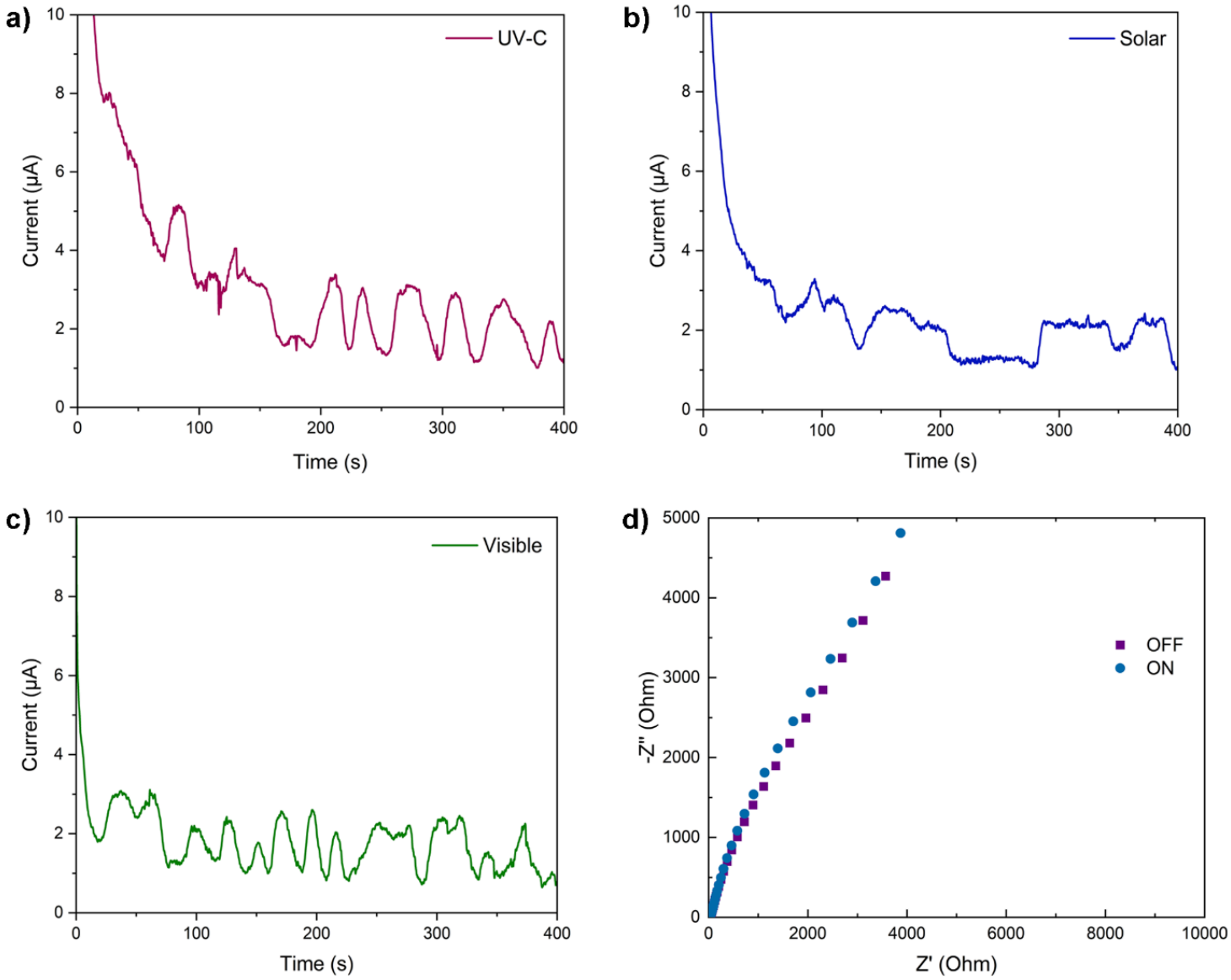


Figure 6

Transient photocurrent response under (a) UV-C, (b) simulated solar, and (c) visible-light irradiation, and (d) Nyquist plots recorded under dark and illuminated conditions.

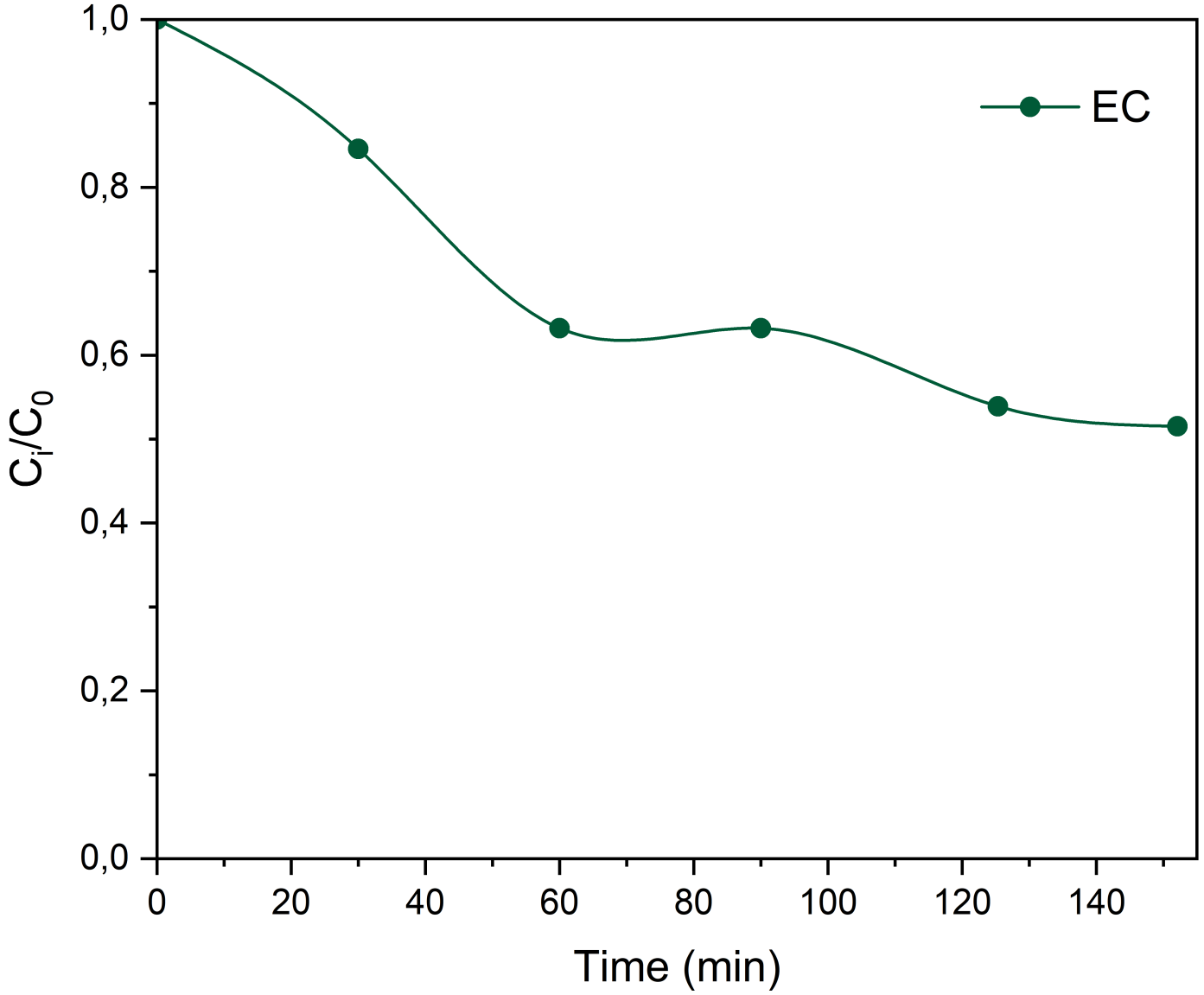


Figure 7

Evolution of normalized CIP concentration during galvanostatic electrochemical oxidation using the TiO_2-functionalized Ti6Al4V electrode.